

A REVISED VIEW OF THE TRANSIENT RADIO SKY

D. A. FRAIL¹, S. R. KULKARNI², E. O. OFEK^{2,3}, G. C. BOWER⁴ & E. NAKAR⁵*Draft of February 9, 2022*

ABSTRACT

We report on a re-analysis of archival data from the Very Large Array for a sample of ten long duration radio transients reported by Bower and others. These transients have an implied all-sky rate that would make them the most common radio transient in the sky and yet most have no quiescent counterparts at other wavelengths and therefore no known progenitor (other than Galactic neutron stars). We find that more than half of these transients are due to rare data artifacts. The remaining sources have lower signal-to-noise ratio (SNR) than initially reported by 1 to 1.5σ . This lowering of SNR matters greatly since the sources are at the threshold. We are unable to decisively account for the differences. By two orthogonal criteria one source appears to be a good detection. Thus the rate of long duration radio transients without optical counterparts is, at best, comparable to that of the class of recently discovered Swift J1644+57 nuclear radio transients. We revisit the known and expected classes of long duration radio transients and conclude that the dynamic radio sky remains a rich area for further exploration. Informed by the experience of past searches for radio transients, we suggest that future surveys pay closer attention to rare data errors and ensure that a wealth of sensitive multi-wavelength data be available in advance of the radio observations and that the radio searches should have assured follow-up resources.

Subject headings: catalogs — radio continuum: galaxies — surveys

1. INTRODUCTION

A century ago, the study of variable stars was a leading area of astronomy. With the increasing availability of large format optical detectors and inexpensive high speed computing this sub-field, as witnessed by projects such as ASAS, OGLE, Catalina Sky Survey, the Palomar Transient Factory, PanSTARRS and SkyMapper, is making a come-back. Radio astronomy appears to be poised for a similar growth. At meter wavelengths, commercially available signal processing chips make it feasible to image the entire primary beam of a dipole or a cluster of dipoles. These technological innovations lie at the heart of LOFAR (Röttgering et al. 2003), MWA (Lonsdale et al. 2009) and LWA (Ellingson et al. 2009). At centimeter wavelengths the “large number, small diameter” (LNSD) array approach (made possible by inexpensive signal processing, advances in commercial RF technology, innovative ideas in the design of small diameter telescopes and phased array focal planes) has now been demonstrated to be a cost effective method of building high speed mapping machines (Welch et al. 2009; Dewdney et al. 2009; Jonas 2009; Oosterloo et al. 2009). The LNSD approach has motivated a new generation of radio facilities: Apertif/WSRT (Oosterloo et al. 2009); MeerKAT (Booth et al. 2009); ASKAP (Johnston et al. 2008).

We divide radio transients into four categories based

on two attributes. The first is the duration of the basic phenomenon (shorter than or greater than a few seconds). The second is their location (within the Galaxy or extra-galactic). Roughly speaking the duration maps to coherent versus incoherent emission and the location to repeated versus cataclysmic events.

Pulsars and related phenomenon (giant pulses, nulling pulsars, erratic pulsars, rotating radio transients, and magnetars) are the dominant category of short duration radio transients at meter and centimeter wavelengths. There are no secure examples of short duration radio transients that are located beyond the local Group. Flare stars and associated phenomena are prime examples of long duration radio transients of Galactic origin.

The focus of this paper is long duration transients of extra-galactic origin. Known examples in this group are supernovae (Weiler et al. 2010) and gamma-ray burst afterglows (Gehrels et al. 2009). In both cases, the radio emission arises as the fast moving debris interacts with the circumstellar matter. In Table 1 we summarize the areal density of radio-emitting supernovae (including the sub-classes) and GRB afterglows. Note the areal density of “live transients” (transients present at any given instant of time) of both supernovae and GRB afterglows is less than 0.05 per square degree.

In 2007, Bower et al. [hereafter, B07] reported on the analysis of a single field observed every week as a part of the Very Large Array (VLA) calibration program. The observations were conducted at 4.8 GHz and 8.4 GHz and lasted 22 years. The 944 epochs and the weekly cadence makes this data set a most valuable set to probe the decimeter band for long duration transients at the sub-millijansky level. These authors reported the discovery of eight transients found in only one epoch (hereafter “single-epoch”; duration, $20 \text{ minutes} < t_{\text{dur}} < 1 \text{ week}$) and two transients found in rolling 2-month searches

¹ National Radio Astronomy Observatory, P.O. Box O, Socorro, NM 87801

² Caltech Optical Observatories 249-17, California Institute of Technology, Pasadena, CA 91125, USA

³ Benoziyo Center for Astrophysics, Faculty of Physics, The Weizmann Institute for Science, Rehovot 76100, Israel

⁴ Astronomy Department, University of California, Berkeley, 601 Campbell Hall #3411, Berkeley, CA 94720-3411, USA

⁵ Raymond and Beverley Sackler School of Physics & Astronomy, Tel Aviv University, Tel Aviv 69978, Israel

TABLE 1
LONG DURATION TRANSIENT POPULATIONS

Class	Rise yr	Decay yr	D	Host mag	Rate deg ⁻²	Ref.
Type II SNe	0.1-1	10	100 Mpc	16	0.04	Gal-Yam et al. (2006)
Type Ib/c SNe	0.1	0.3	50 Mpc	14.5	5×10^{-6}	Berger et al. (2003)
SN1998bw-like	0.1	0.1	300 Mpc	18.4	3×10^{-4}	Soderberg et al. (2006)
Sw J1644+57-like	0.1	1	$z \sim 1.8$	21.7	0.1	Zauderer et al. (2011)
Orphan Afterglows	1	1	1 Gpc	21.0	10^{-2}	Levinson et al. (2002)
NS-NS mergers	0.1-1	0.1-3	800 Mpc	20.5	5×10^{-3}	Nakar & Piran (2011)

NOTE. — Detectability distance and rates have been calculated assuming a single snapshot at a flux density threshold of 0.3 mJy. See section 5 for details. D is the distance at which the typical transient will have a specific flux of 0.3 mJy. Host is the apparent magnitude of a galaxy with -19 absolute magnitude at distance D .

(hereafter, “multi-epoch” sources).

Deep observations towards these sources were undertaken at optical, near-IR and X-ray bands. The most remarkable feature of the B07 sources is an absence of optical and near-IR counterparts, despite deep searches (B07; Ofek et al. 2010). As noted by Ofek et al. (2010) all extra-galactic transients (regardless of the band at which the transient was discovered) have detectable optical counterparts, namely, their host galaxies. Furthermore, remarkably the areal density of transients live at any given time was estimated to be 1.5 deg^{-2} ($S > 0.37 \text{ mJy}$). This density exceeds that of all other known radio transient source populations by an order of magnitude (or more); see Table 1. Ofek et al. (2010) thus argued that the absence of an optical counterpart means that B07 transients have to be repeating sources of Galactic origin, and proposed that B07 transients are old neutron stars (which naturally satisfy the requirement of being optically almost invisible).

Given that the search for transient and strong variables is one of the primary motivators for the next generation radio facilities (described earlier) it is important to critically investigate the B07 transients since this class nominally dominates over all other known classes of radio transients (see Table 1). To this end, here we report on a re-analysis of the original data of B07 (§2, §3) and revisit the transient reported by Ofek et al. 2011 (§3.8). In §5 we present an update of the expected rate of radio transients. In §6 we discuss these rates in relation to future synoptic radio imaging surveys and conclude.

2. OBSERVATIONS AND RE-ANALYSIS

The data used by B07 arose from a calibrator program carried out during the period 1983–2005. All observations were made in the standard continuum mode with 100 MHz of total bandwidth in each of two adjacent 50-MHz bands (IFs) at center frequencies of 5 GHz and 8.4 GHz and in both hands of circular polarization. See B07 for more details about the full data-set.

For the re-analysis we selected, from the archive, only the raw data relevant to the transients reported in B07. This means the eight epochs from which the single-epoch transients were first found and the 3+8 data sets from which the two multi-epoch transients were found. Data were taken at other radio frequencies in about half of the cases. Some details of the single epoch and two-month transients can be found in Table 2).

For the re-analysis we used AIPS⁶ (Greisen 2003). The data reduction and imaging followed the same path used by B07 with a small exception. B07 employed AIPS for the flagging and analysis of the single-epoch transients, and used the *Miriad* package (Sault et al. 1995) for imaging the two-month averages. We endeavored to make the calibration and the flagging of UV data (AIPS task TVFLG) data for each epoch as uniform way. Following these steps we ran each raw visibility data set through the VLA pipeline (VLARUN).

No flux density calibrator was observed during any epoch of these test observations. Following B07, the flux density of the phase calibrator (B1803+784) was fixed to be 2.2 Jy (5 GHz) and 2.8 Jy (8.4 GHz). For those epochs with 22 GHz and 1.4 GHz observations the flux density of the phase calibrator was taken to be 3 Jy and 2 Jy, respectively. It is evident from the strong variations in the radio light curves for B1803+784⁷ that these mean values are only approximate. Our reinvestigation confirm that at least during the period 1981–1999 the variation was less than 15%. Fortunately, an accurate flux density scale is not crucial for our analysis since we report results in terms of the signal-to-noise.

Following B07 we applied a Gaussian weighting to the visibility data in order to limit the effects of bandwidth smearing. This was done by applying a 150-kλ taper to all visibility data prior to imaging (IMAGR). For each field we required that a source be present in both frequency bands (IFs) with similar flux densities and with similar positions. Images were made with extra large fields-of-view. The wide field-of-view is necessary to reduce the effect of side-lobes that can mimic sources in narrow fields. These final analysis images had a size of about 40-arcmin at 5 GHz data and 27-arcmin at 8.4 GHz. For guidance, the full-width at half power for VLA antennas is 45-arcmin/ ν (GHz), or 9.3-arcmin at 5 GHz and 4.3-arcmin for 8.4 GHz. Measurements of the VLA beam power response beyond the first null are given in Cotton and Perley (2010), while the polynomial coefficients needed to correct for the primary beam attenuation can be found in the AIPS task PBCOR. We do note that these corrections are uncertain for large angular distances from the beam center. All data were taken in the B1950 coordinate system. We stayed in the B1950 sys-

⁶ <http://www.aips.nrao.edu/>

⁷ U. Michigan Radio Astronomy Observatory database

tem throughout calibration and imaging.

3. FINDINGS

Below we offer a detailed report for each of the ten sources reported in B07. Summarizing our results for the impatient reader we find four of the eight single-epoch transients [RT 19840502 (§3.1), RT 19860122 (§3.4), RT 19840613 (§3.2), RT 19860115 (§3.3)] and one of the two-month transients (RT 19870422; §3.5) to be artifacts. Our re-analysis finds that the remaining long-duration transient, RT 20010331 (§3.6) did not have a significant detection when imaged with AIPS (SNR of 3.2) but the *Miriad* imaging yields an SNR of 7.4.

For the remaining single epoch sources [RT 19920826, RT 19970205, RT 19970528, RT 19990504] our analysis (undertaken by DAF; see §2 for a summary of our data reduction) finds reduced SNR. The discrepancy with respect to the results reported in B07 concerned us and so another author (GB) reanalyzed these fields. Some of the discrepancies arise from UV data flagging but even when the same flagging is used different SNR algorithms yield measures which differ by 1 to 1.5σ . Since the sources lie close to threshold of detection even a small shift of a single σ has an exponential effect in their confidence. In effect, the reality of this group (taken as a whole) apparently depends on details of algorithms in AIPS and *Miriad* – the investigation of which is beyond the scope of this paper. Below in §3.7.1–3.7.3 we detail the analyses and a summary of the SNRs of these sources can be found in Table 2.

We also re-investigated the lone transient candidate reported in Ofek et al. (2011). Our re-examination which now correctly includes the number of independent beams that were searched for shows that there is a four percent probability that this candidate is due to noise (see §3.8). In the next section (§4) we synthesize these findings and present our conclusions about the B07 transients.

3.1. RT 19840502

B07 report finding a transient close to the pointing center ($13''$) with a primary beam-corrected flux density of $448 \pm 74 \mu\text{Jy}$, or a $\text{SNR}=6.1$. We imaged the calibrated data set and confirmed the presence of emission at this level at the reported position. However, we identified a phase center artifact in the visibility data for the left hand polarization of the upper IF band. The effect of this artifact in the image plane is to create strong positive and negative sidelobes, with the positive feature identified as a transient source (Figure 1). When the upper IF band data are removed the resulting image is noise-like and the peak flux density at the nominal position of the reported transient is $191 \pm 97 \mu\text{Jy}$. Additional observations were taken during the same epoch at 15 GHz. The peak flux density at the same position is $-243 \pm 200 \mu\text{Jy}$.

3.2. RT 19840613

B07 report finding a transient coincident with a possible host galaxy ($z = 0.040$) and with a primary beam-corrected flux density of $566 \pm 81 \mu\text{Jy}$, or a $\text{SNR}=7.0$. Our deconvolved image shows a source at that location. Gaussian fitting suggests that the source is resolved and this conclusion is supported with an integrated flux density ($715 \pm 218 \mu\text{Jy}$) being clearly larger than the estimate of the peak flux density of $388 \pm 82 \mu\text{Jy}$. Imaging

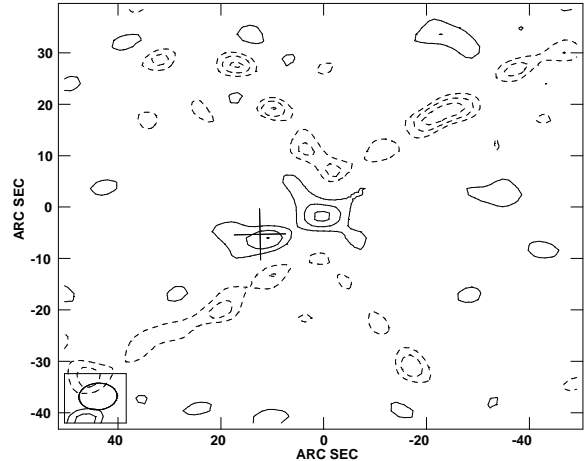


FIG. 1.— Image of RT 19840502 marked by cross. The feature at the center (0,0) is an artifact (“phase center”). Once the bad visibility data is removed the transient candidate is not visible on the final image. Contours are displayed in steps from -1 , -0.75 , -0.5 , 0.5 , 1.0 , 1.5 mJy , with negative (positive) contours given by dashed (solid) lines. The synthesized beam size is shown in the lower left.

the lower and upper IFs separately we find another discrepancy. The peak flux density in the lower IF is four times weaker than the upper IF band.

The likely source of the problem can be seen by comparing the dirty image with the dirty beam (Figure 2). RT 19840613 appears to be an uncleaned side-lobe of J150123+781806, one of the brighter persistent sources detected in 452 images made by B07 at 5 GHz. The putative transient is $56''$ away from J150123+781806 to the northwest, close to a local maximum (10% of peak) in the dirty beam at this location. This side-lobe artifact is stronger in the upper band but it is still present in the lower band.

Deconvolution does not fully remove the side-lobe from the image and the effect is to produce a false transient. We investigated whether the artifact is due to short-timescale ($\sim 10 \text{ min}$) variability of J150123+781806 but after dividing the visibility data in half (by time) and re-imaging, we found no evidence for variability. The artifact may be due to some low level interference picked up by some antennas baselines but we were not able to identify the bad data. It is possible that RT 19840613 is a real transient that unfortunately lies on the side-lobe of the dirty beam, but its Gaussian fit parameters and its variation in the lower and upper sidebands suggest that it is not a real source.

Additional observations were made during this epoch at 1.5 GHz. The data quality is good and the images have no obvious artifacts. No source is visible at the transient position. The peak flux density is $133 \pm 113 \mu\text{Jy}$.

3.3. RT 19860115

B07 report a transient with a primary beam-corrected flux density of $370 \pm 67 \mu\text{Jy}$, or a $\text{SNR}=5.5$. Some of the same issues with the image of the previously discussed RT 19840613 were also seen for RT 19860115. In

TABLE 2
SINGLE EPOCH AND TWO-MONTH TRANSIENT CANDIDATES

Name Candidate	Type	Freq. (GHz)	FWHM/2 (arcmin)	$\Delta\theta$ (arcmin)	Beam (arcsec)	Notes
RT 19840502	SE	4.9	4.6	0.22	6.0	Phase center artifact.
RT 19840613	SE	4.9	4.6	3.3	5.7	Side-lobe of bright source.
RT 19860115	SE	4.9	4.6	1.3	14.8	Side-lobe of bright source.
RT 19860122	SE	4.9	4.6	4.6	14.5	Artifact. Lower IF is bad.
RT 19870422	2M	4.9	4.6	8.0	12.8	Artifact. Bad pointing.
RT 20010331	2M	8.5	2.6	4.4	1.5	No detection (see §3.6).
RT 19920826	SE	4.9	4.6	2.0	21.2	D SNR: 6.4; 5.8.
RT 19970205	SE	8.5	2.6	4.4	1.4	B SNR: 7.7; 5.7 (CA)
RT 19970528	SE	4.9	4.6	6.8	3.9	CnB SNR: 7.5; 5.6. (CA)
RT 19990504	SE	4.9	4.6	8.9	18.9	D SNR: 7.3; 5.7.
RT 19970528	SE	8.5	2.6	6.8	1.3	CnB No detection (BA)
RT 19990504	SE	8.5	2.6	8.9	8.3	D No detection (BA)

NOTE. — Starting from the left the columns are as follows. The name of the transient as RTYYYYMMDD where YYYY is the UT year, MM is the month index and DD is the day number at which the transient was first detected; the type of transient: single epoch (SE) or two month average (2M); the center frequency in GHz; one half of the full-width at half-maximum of the primary response beam in arc minutes; the offset of the transient from the phase center, also in arc minutes; the beam size in arc seconds computed as geometric mean of the major and minor axes. The last column report the array configuration, two SNRs (for sources detected and reported as such in B07) and some comments. The left SNR (in *italics*) are the SNR from B07 and the right SNR (in **typewriter** font) are SNR resulting from the work presented here (see §3 for details). The comments are as follows: CA for severe Chromatic Aberration and BA for severe Beam Attenuation. The first group of transients are either artifacts or clearly very low SNR. Following that (separated by a line) are four transients which are threshold sources. The last group is composed of higher frequency observations of two of these threshold sources and given the strong beam attenuation there was no expectation of detection. The entries were made merely for completeness.

Figure 3 we show the dirty image along with the synthesized beam. The RT 19860115 appears to be an uncleaned side-lobe of J150123+781806 and hence not a real transient. RT 19860115 lies at the same angular distance (3.3') and position angle (100° CCW CC) of a local maximum in the side-lobe structure (25% of the peak beam). We were unable to identify the source of these strong side-lobes. As in the case of RT 19840613, we were able to rule out that the strong side-lobes originated from short-term variability of J150123+781806.

3.4. RT 19860122

B07 report a transient with a primary beam-corrected flux density of $1586 \pm 248 \mu\text{Jy}$, or a SNR=6.4. Images made with all the visibility data do show emission at the position of RT 19860122 with the reported peak flux density. However, there does appear to be some erroneous visibility data resulting in low-level rings in the image centered at the phase center. The bad data were traced to the lower IF. If the data for the lower IF band are removed there is no source at the reported transient position (peak flux density of $303 \pm 189 \mu\text{Jy}$).

3.5. RT 19870422

This is one of two transients found by binning individual epochs into two-month averages. B07 report a 5 GHz transient with a primary beam-corrected flux density of $505 \pm 83 \mu\text{Jy}$, or a SNR of 6.1. The source J150050+780945.5 is positionally coincident with a blue host galaxy ($z = 0.249$) and has been suggested by Nakar & Piran (2011) as a candidate afterglow from a binary coalescence event. Three single epochs were used to form the average. They are in YYYYYMMDD format: 19870414, 19870422 and 19870429. A close inspection of

the data reveals a problem. The last two of the three epochs used to find RT 19870422 were pointed to a different part of the sky, an error that was made when the original observing files were written. The source is actually J210133.67+373528, and appears only as a transient when added inappropriately to the data from the standard on-the-sky test field. In hindsight we recognize these to be the same type of errors as seen earlier (see Ofek et al. 2010).

3.6. RT 20010331

This is the second of the transients which were found by binning individual epochs into two-month averages. B07 report a 5 GHz transient with a primary beam-corrected flux density of $697 \pm 94 \mu\text{Jy}$, or a SNR=7.4. Separately, Croft et al. (2011) reported a marginal X-ray source at this position.

Eight single epochs were used to form the average. They are in YYYYYMMDD format: 20010306, 20010314, 20010321, 20010328, 20010403, 20010411, 20010418 and 20010425. We calibrated and imaged the eight epochs of observations from 2001 March 6 to 2001 April 25 (all in B-configuration). While the four quiescent sources from B07 can be seen in this deep image, we do not identify a significant source at the position of RT 20010331. The brightest peak within the synthesized beam (natural weighting) is $42 \pm 13 \mu\text{Jy}$ (or 3.2σ). An independent reduction using the AIPS package by GB confirms the absence of this source.

The first problem lies with the primary beam corrections reported in B07. RT 20010331 lies 4.4' from the phase center, close to the 10% response radius of the primary beam. Our estimate for the rms noise of $13 \mu\text{Jy}$ lies within a few percent of the theoretical value. The beam-corrected rms noise in this case (at 10% response

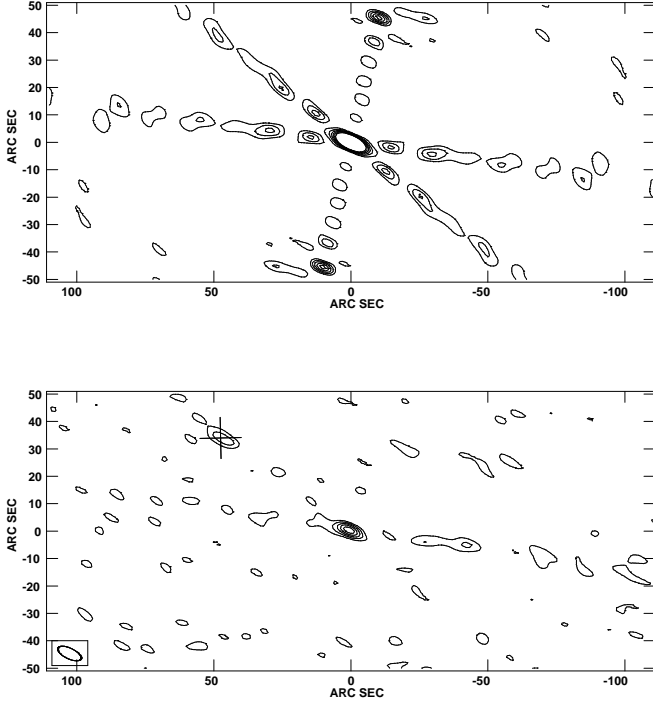


FIG. 2.— *Top*: The dirty beam for the RT19840613 field. This sub-image shows the northwestern side of the beam. The peak is located in the lower right hand corner. The contours are 5, 10, 15, 20, 25 and 30% of the peak flux. *Bottom*: The dirty image toward RT19840613. A cross marks the location of transient. Contours are 0.13, 0.23, 0.33, 0.43, 0.53, 0.63 mJy beam⁻¹. Note that the transient candidate RT19840613 lies at the same angle and position as a side-lobe from the bright source J150123+781806 located in the bottom right corner of this image.

of the primary beam) would then be about 129 μ Jy, not the 94 μ Jy given in B07. Rather than correcting at the 10% radius, it appears that the flux density and noise in B07 were mistakenly corrected at the 14% power level. This multiplicative error has no impact on the signal-to-noise.

In order to investigate this signal-to-noise discrepancy between our image and B07, we split the data in various ways (separate epochs, months of March and April epochs, adjacent IF bands) and re-imaged, looking for a bright peak. None were found.

The discrepancy between B07 and the work reported apparently can be traced back to differences in the *Miriad* and AIPS imaging packages. Our calibrated visibility data, when processed through *Miriad* using nearly identical imaging parameters as those in AIPS, gives a flux density of $91 \pm 13 \mu$ Jy (7σ). We have no explanation for the discrepancy between the two results obtained from AIPS and *Miriad*. It is worth noting that the peak flux densities of the persistent sources identified by B07 agree in these images to 0.5σ . For this paper we accept the analysis given here.

There was one epoch (2001 March 6) in which data were also taken at 5 GHz. The peak flux density at the position of RT 20010331 is $-27 \pm 39 \mu$ Jy. In summary,

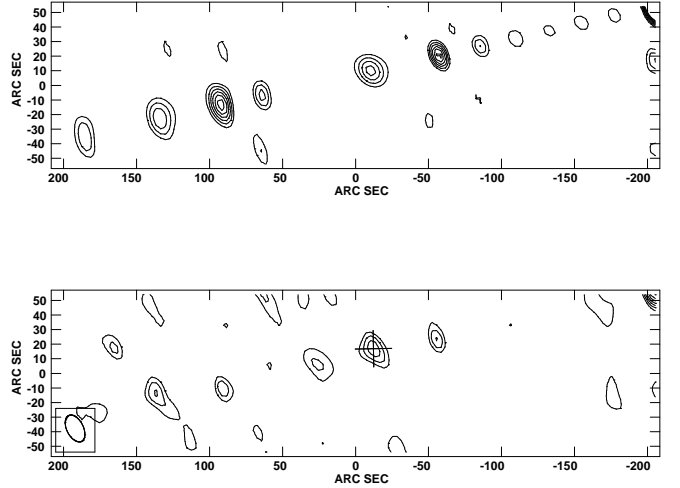


FIG. 3.— *Top*: The dirty beam for the RT19860115 field. This sub-image shows the southwestern side of the beam. The peak of the beam is located in the upper right hand corner. The contours are 7.5, 12.5, 17.5, and further in steps of 5% up to 37.5% of the peak flux. *Bottom*: Dirty image toward RT19860115. A cross marks the location of the transient. The contours are 0.15, 0.25, 0.35, 0.45, 0.55, 0.65 and 0.75 mJy beam⁻¹. Note that the transient candidate RT 19860115 lies at the same angle and position as a side-lobe from the bright source J150123+781806 located in the upper right corner of this image.

we find no evidence to support that RT 20010331 is a significant detection.

3.7. Remaining Four Single Epoch Sources

3.7.1. RT 19920826

B07 report a transient with a primary beam-corrected flux density of $642 \pm 101 \mu$ Jy, or a SNR=6.4. We confirm a source at this position but with a slightly reduced SNR. Using natural weighting of the gridded visibilities, our measured peak flux density is $460 \pm 80 \mu$ Jy, or 5.8σ . Despite the lower significance, there is some confidence that RT 19920826 is real since it appears in both IFs with comparable flux densities. Further investigation by GB shows that the difference in the SNR between B07 and the analysis here can be traced to differences in flagging of the UV data (of two specific antennas).

3.7.2. RT 19970528

B07 report a transient with a primary beam-corrected flux density of $1731 \pm 232 \mu$ Jy, or a SNR=7.5. These observations were taken during a time when some antennas were being moved to the B configuration and so we applied antenna position corrections (via AIPS task VLANT) before calibration.

RT 19970528 is $6.8'$ from the center of the image, where the response of the antennas is only 16% of their peak. The uncorrected flux density is 270 ± 47 . A point source search (AIPS task SAD) of the four million pixels enclosed interior to a radius around this candidate, shows six other un-cataloged candidates with similar signal-to-noise. The primary-beam corrected flux density

1.7 ± 0.3 mJy is similar that from to B07. This estimate does not include a correction for temporal smearing due to the sources distance from the phase center, nor for the added uncertainty in the magnitude of the primary beam correction beyond the 20% point. Correcting for these terms we get 2.8 ± 0.5 mJy.

GB re-investigated this source and found that with the B07 analysis the SNR varies with the approach (peak/rms, SAD, JMFIT) between 6.2, 7.4 and 7.1. (without any corrections discussed above). The corresponding SNRs for the image discussed above is 6.1, 5.1 and 6.8. The source is a bit “ratty” and this may explain the variation in SNR. We therefore find this source to be a weak detection.

Additional observations were made during this epoch at 8.5 GHz. The source lies close to the first null ($6.4 \pm 0.3'$ from the phase center) of the beam at this frequency. The attenuation by the primary beam is severe and hence the sensitivity is not sufficient to provide any strong spectral index constraints.

3.7.3. RT 19990504

B07 report a transient with a primary beam-corrected flux density of $7042 \pm 963 \mu\text{Jy}$, or a SNR=7.3. Croft et al. (2011) report an X-ray source in the vicinity of the radio source. Deep multi-wavelength data is consistent with the X-ray source arising from a QSO but located five arcseconds from the putative radio transient.

We find the (uncorrected) peak flux density is $290 \pm 51 \mu\text{Jy}$ (or an SNR of 5.7). RT 19990504 lies $8.9'$ from the phase center, close to the first null ($11.1 \pm 0.6'$ from the phase center) where we would not expect to find sources. The polynomial expressions used in AIPS to correct for the beam attenuation are increasingly inaccurate outside the 20% response radius, and they are not applicable close to the null. The azimuthally averaged measured value of the beam response is 1.8%, implying a flux density correction factor of $55\times$ (Cotton and Perley 2010) or 16.0 ± 2.8 mJy.

As with RT 19970528, the analysis of B07 data by GB finds SNR of 5.6 (peak/rms), 7.3 (SAD) and 6.8 (JMFIT) and a similar variation with the image reported here. It is worth noting that the source may be extended and also that a visual inspection of the annular region reveal a number of similar sources. We conclude that RT 19990504 is not a robust detection.

Additional observations were made during this epoch at 8.5 GHz. An image was made from these higher frequency data but, as expected, no source was found.

3.7.4. RT 19970205

This is the only single-epoch transient identified at 8.5 GHz by B07. They report a primary beam-corrected flux density of $2234 \pm 288 \mu\text{Jy}$, or a SNR=7.8. RT 19970205 is $4.4'$ from the center of the image, where the response of the antennas is only 9.8% of their peak. There is an elongated source at this position with a peak flux density of $231 \pm 41 \mu\text{Jy}$ (using natural weighting). There is some indication that the source is extended since the integrated flux density is about twice the peak flux density.

The peak flux density was likely underestimated by B07 since they did not fully correct for bandwidth or temporal smearing effects. These data were taken in the

BnA array with an integration time of 3 1/3 s and a 50-MHz bandwidth. In this observing configuration, the effects of temporal smearing with this dump time will likely reduce the peak flux density by only a few percent. However, chromatic aberration is expected to be larger with the effect of smearing a point source along the radial direction (Perley et al. 1989).

Accounting for the bandwidth effect, we measure a peak flux density of 3.4 ± 0.6 mJy (SNR=5.7). Next, due to the uncertainty about the form of the primary response function beyond the 20% point (AIPS task PB-COR), we only know that the peak flux of RT 19970205 lies in the range of 2.9–4.4 mJy. As noted above the source is likely extended and this may account for the variation in SNR (from ≈ 6 to 7.6).

3.8. Other Surveys

Ofek et al. (2011) presented a survey for 5 GHz radio transients at low Galactic latitudes. Most of the data were reduced in near-real time (2 hr delay) and transient candidates were followed up with radio, visible light and X-ray instruments. The authors reported a single transient candidate, J213622.04 + 415920.3 with a peak specific flux of 2.36 ± 0.41 mJy (5.8σ) and with no obvious optical counterpart.

We have re-analyzed this data set and confirm that the SNR is 5.8. Considering that the search resulted from inspecting 1.1×10^7 independent beams (§D) and assuming Gaussian statistics, we find that the probability of the highest event found in these many independent beams is attributable to chance or noise is 3.6% (see §A). Therefore, we advocate that this candidate is not a real event.

4. THE REVISED B07 TRANSIENT RATE

As noted in §1 the ten transients reported in B07 were remarkable for their apparent abundance (1.5 per square degree, at any given epoch) *and* the lack of quiescent optical counterparts. In §3 we found that five of the B07 transients are artifacts arising out of (rare) data acquisition problems or imaging artifacts (see Table 2). We find that the 2-month transient RT 20010331 is not well detected. We argue that the single transient reported by Ofek et al. (2011) is also not a robust detection.

In §3 we present our analysis for the remaining four transients (all of which are single-epoch transients): RT 19920826, RT 19970205, RT 19970508 and RT 19990504. We find SNRs which are typically 1- σ below that reported in B07. The revised and B07 SNRs are given in Table 2. We note that an independent pipeline written in ParselTongue (Kettenis et al. 2006), a Python interface to AIPS, and run on three of these four sources confirms the lower SNR values found here (Bell 2011): RT 19920826 (SNR=6.0), RT 19970528 (SNR=4.4), and RT 19990504 (SNR=4.0).

The lowering of SNR (from between 7 and 8 to between 5 and 6) has a pernicious effect when the number of independent beams which were search is included. In §D we estimate this number to be $n \approx 9 \times 10^7$. In §A we derive the probability density function for the highest m values of n Gaussian random numbers⁸. In Figure 4 we plot the

⁸ Theory informs us that the statistics of beam values or equiv-

density function for the highest value ($m = 1$) and the fourth highest value ($m = 4$). As can be seen from this Figure 4, if the SNRs reported here are accepted then the global case for the remaining B07 transients is entirely weakened. If, on the other hand, the SNRs reported in B07 are accepted then the four transients reported in B07 do argue for a new class of radio transients.

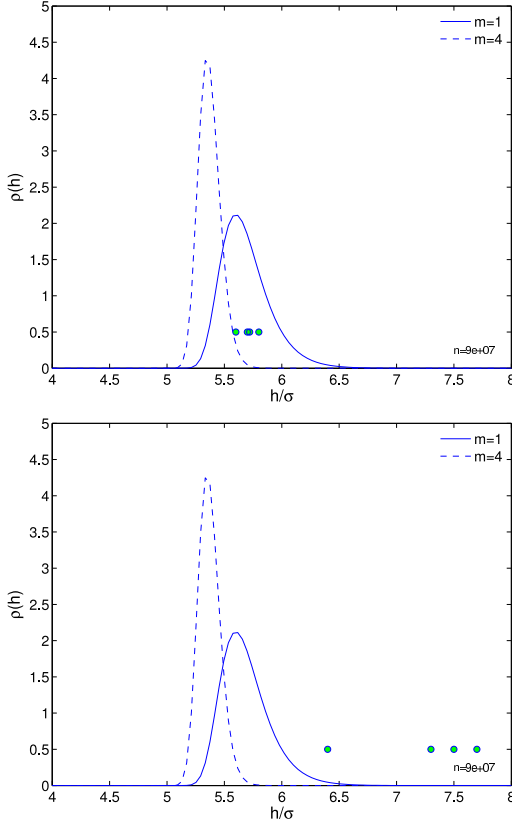


FIG. 4.— The probability density function of the highest value ($m = 1$) and the fourth highest value ($m = 4$) of a population of $n = 9 \times 10^7$ Gaussianly distributed random numbers with zero mean and unit variance. The probability density function plotted here is discussed in §A and the justification for n can be found in §D. The dots represent the SNRs of the following single-epoch transients discussed in Table 2. (from left to right): RT 19905054, RT 19920826, RT 19970205 and RT 19970228. (Top): SNRs as reported in this paper. (Bottom): SNRs as reported in B07. Note that the vertical location of the dots is arbitrary. For details of these density distributions see §A.

The above approach of using a fixed threshold for all epochs does not result in optimal detection. In particular, the threshold for a low resolution survey is lower than that for a higher resolution survey (since the latter has a correspondingly larger number of synthesized beams). B07 addressed this problem by requiring that the probability of a false detection (PFD) in an individual epoch was constant and less than N where N is the total number of images. With this approach, the expectation number of false detections is 1 for the entire survey. Applying the B07 method we find the following PFDs:

alently pixel values of interferometric maps should follow Gaussian distribution.

RT 19920826 ($\log(\text{PFD}) = -5.02$); RT 19970205 (-2.74); RT 19970528 (-2.77); RT 19990504 (-4.61). With this more refined approach only RT 19920826 and 19990504 survive. However, for reasons discussed in §3.7.3 we have misgivings about RT 1990504.

An entirely different approach⁹ (and in some ways orthogonal to the above SNR based approach) is to look at the angular distribution of the transient sources with respect to the primary axis¹⁰. Basic interferometry theory informs us that the dirty image is simply the Fourier transform of the visibility data. As such the radiometric noise in the dirty image should be independent of the angular offset from the phase center. In contrast, the point source sensitivity decreases as one goes away from the pointing center and this is governed by the primary beam response (assuming that the spectral resolution of the survey is high enough that the delay beam is larger than the primary beam). Thus, once the minimum SNR for detection is fixed, cosmic sources should be concentrated towards the pointing direction whereas noise spikes (masquerading as threshold point sources) should be uniformly distributed.

In §B we derive the expected distribution of cosmic sources as a function of the angular offset. In Figure 5 we plot the expected cumulative distribution and also the angular offset of the four sources which are not artifacts but whose SNR seems to be under dispute, namely RT 19920826 (§3.7.1), RT 19970205 (§3.7.4), RT 19970528 (§3.7.2) and RT 19990504 (§3.7.3). From this Figure one can see that only RT 19920826 lies in the expected region whereas the remaining three are collectively improbable.

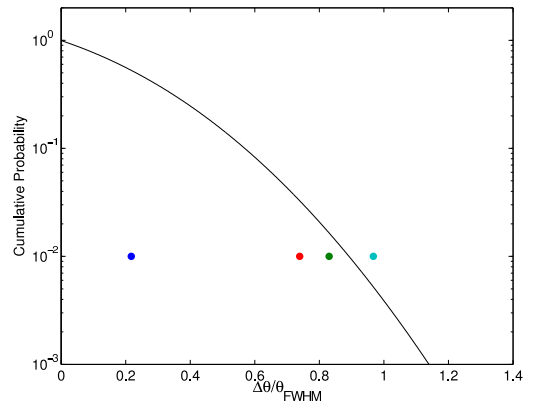


FIG. 5.— The cumulative probability of finding a cosmic source (but integrated from angular offset of infinity to zero) as a function of the angular offset with respect to the pointing center. The angular offset is normalized in units of θ_{FWHM} . The sources are represented by dots and are (from left to right): RT 19920826, RT 19970528, RT 19970205, and RT 19990504. The points are deliberately placed at cumulative probability of 1%. RT 19920826 is firmly within the region where one naturally expects cosmic sources.

In summary, two different statistical tests, one based on SNR and the other making use of the spatial signa-

⁹ This test was recommended to us by J. Condon.

¹⁰ We assume that all antennas are pointed in the same direction and this direction is both the pointing axis as well as the phase center.

ture provided by the primary beam, suggest that of the remaining four sources detected at threshold, only one, namely, RT 19920826 is a good detection. Thus a simple interpretation of our re-analysis is that the rate of B07 transients is considerably lower than that reported by B07, perhaps an order of magnitude smaller.

We acknowledge that the discrepancy between the analysis presented in B07 and the analysis presented here (and re-investigated) is disturbing. In the previous section (§3.7) we investigate the reasons for the discrepancy in the SNRs and variously find possible and plausible causes: flagging of data, the choice of data reduction package (AIPS versus *Miriad*) and the specific method used to compute SNRs. However, none of these explanations are satisfactory. We are continuing this investigation but at the present time we consider this topic to be beyond the scope of the paper.

In contrast, the sources which we find as artifacts have ready explanations (see Table 2). One source is a result of the file header containing a pointing direction of the previous pointing. Another is due to a systematic associated with local signals (RFI). These signals do not have the natural fringe rate of cosmic sources and appear as candidates close to the phase center. Two are side-lobes of a stronger sources.¹¹ Suffice to say that such rare errors will be found if one inspects sufficiently large number of beams!

5. A REVISED LOOK AT THE TRANSIENT RADIO SKY

In Figure 6 we plot the areal densities of three known transients (SN1998bw-like, type-II RSN and Swift J1644+57-like) and that of two expected classes (NS-NS mergers and orphan afterglows of long duration GRBs) of transients. The areal density of these five classes is also summarized in Table 1. We briefly discuss each of these five classes of transients below.

The traditional extra-galactic radio transients are type II radio supernovae. The rate that we present here is based on the single radio SN detected in a blind radio survey by Gal-Yam et al. (2006) and it agrees with an independent estimate by Lien et al. (2011). As illustrated by the example presented in Gal-Yam et al. (2006), the main advantage in the search for radio SNe in a blind survey is the unique view that it provides to the otherwise hidden population of heavily obscured SNe. The observed rate of other types of radio SNe (e.g. ordinary type Ib/c SNe) are considerably lower than that of type II supernovae and are not discussed further.

Radio emission is expected from both classical long duration gamma-ray bursts (GRBs) as well as the more abundant but less luminous GRBs exemplified by GRB 980425 associated with the energetic SN Ic supernova, SN 1998bw (Galama et al. 1998; Kulkarni et al. 1998). The radio emission is far brighter than that of ordinary core collapse SN (II, Ib, Ic) and the increased volume makes up for the intrinsically smaller birth rate. The recent discovery of the energetic supernova SN2009bb (Soderberg et al. 2010) demonstrates that radio surveys

can find such sources without resorting to high energy (gamma-ray) missions.

Levinson et al. (2002) estimated the number of afterglows from classical GRBs and whose explosion axis is directed away from us (“orphan” afterglows). The expected rate depends strongly on the poorly constrained γ -ray beaming. On one hand this makes any rate prediction uncertain. On the other hand, even a non-detection by the kind of survey that we discuss below will provide an independent and unique constraint on the average opening angle of long gamma-ray bursts, their true rate and total energy output (Rossi et al. 2008; Nakar et al. 2002; Totani & Panaitescu 2002). The areal density in Figure 6 is derived using a typical opening angle of 10 degrees.

A surprising and apparently an important development in the field of radio transients took place just this year with the discovery of a radio transient associated with the nucleus of a modest size galaxy. The source, Swift J1644+57 was initially detected as a hard X-ray transient (Burrows et al. 2011). Subsequent follow up found a bright, compact self-absorbed radio counterpart, localized at the center of a normal galaxy at $z = 0.354$ (Zauderer et al. 2011; Levan et al. 2011). The current view is that Swift J1644+57 arose from a relativistic jet produced when a star was tidally disrupted as it passed too close to an otherwise dormant super-massive nuclear black hole (e.g. Bloom et al. 2011). Shortly, thereafter, a second candidate non-thermal tidal disruption event (TDE) was recently proposed (Cenko et al. 2011). Events such as these give us an opportunity to study the activity of 10^7 - $10^8 M_\odot$ supermassive black holes in otherwise normal galaxies.

The areal density in Figure 6 is calculated assuming an observed rate of 0.2 yr^{-1} Swift J1644+57-like events and a gamma-ray beaming factor of 10^3 (Zauderer et al. 2011; Bloom et al. 2011). Nominally, Swift J1644+57-like sources appear to be the most frequent extra-galactic transients that will be found in radio transient searches. We acknowledge that the uncertainty of both the observed rate and the gamma-ray beaming is high and the true rate may be significantly different.¹²

Now we come to the most uncertain as well as potentially the most important extra-galactic radio transient – the merger of two neutron stars (or a black hole and a neutron star). It is generally accepted (or expected) that short hard bursts are on-axis explosions of these mergers (Nakar 2007; Metzger & Berger 2011). As in long duration GRBs, radio emission is expected by afterglow (on-axis or orphan). The rates are highly uncertain because there are very few observations of short hard GRBs. Thus there still continues to be a debate about the geometry of these explosions (“jetted” or not). Next, while the expected radio emission is straightforward to estimate (subject to the usual parametric uncertainties of the energy fractions of relativistic electrons and magnetic field) an additional uncertainty is the density of the ambient gas (which is necessary for the production of the afterglow emission).

¹¹ Unfortunately, side-lobes are the exception to the expectation of Gaussian statistics for interferometric images. It is said that “the Central Limit theorem covers a large number of sins but not all sins.”

¹² Estimates based on theoretically predicted TDE rates and luminosities (Giannios & Metzger 2011; Bower 2011; van Velzen et al. 2011) result in areal densities that vary by three orders of magnitude. The rate that we predict here is consistent with the upper range of these predictions.

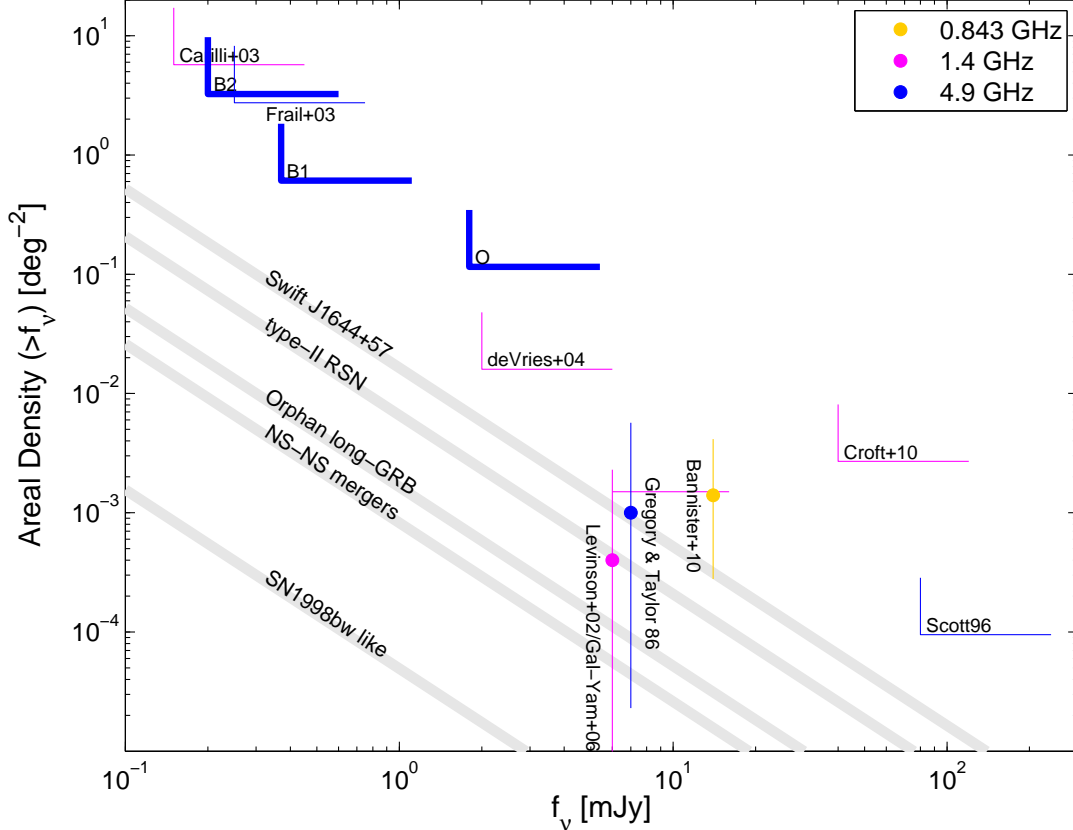


FIG. 6.— Cumulative areal density of transients as a function of peak flux density for all major transient surveys. Most of the surveys are upper limits and the allowed phase space is above and to the right of the L-shaped symbol. The three dark blue L’s (annotated as B2 for the 2-month transients from B07, B1 for the single-epoch transients from B07 and O for the lone transient reported in Ofek et al. 2011) are the upper limits derived as a result of the analysis presented here. These limits were derived by assuming no detection (whence a Poisson upper limit of 3 at the 95% confidence level; see §C) and survey areas summarized in Ofek et al. (2010).

Regardless of the uncertainty whether neutron star mergers are the sources of short GRBs or not, a substantial sub- and mildly relativistic outflow is expected to be ejected during the merger. Nakar & Piran (2011) estimate radio emission from these outflows. The areal density in Figure 6 is calculated based on their estimates¹³, assuming a NS-NS merger rate of $300 \text{ Gpc}^{-3} \text{ yr}^{-1}$ and that any merger ejects 10^{50} erg of a mildly relativistic outflow. We note that Nakar & Piran (2011) suggested that RT 19870422 was the radio emission from the remains of a neutron star merger. However, as noted in §3 this source is an artifact.

6. WAY FORWARD: NEW SURVEYS

There are sound reasons to continue the exploration of the dynamic radio sky. Radio searches are an ideal way to discover core-collapse supernovae embedded in or behind dusty regions. The discovery of SN 2009bb shows that large radio searches can find urgently needed additional examples of nearby low luminosity GRBs. Next, the many rewards of radio follow up observations of

Swift 1644+57 (accurate localization, energetics, beaming, outflow velocity) show the tremendous diagnostic power of radio observations of this entirely new class of extragalactic transients.

As exciting as these developments are, the search for new classes of radio transients has involved several false starts. The euphoria that followed the discovery of a highly dispersed (and therefore argued to be of extragalactic origin) millisecond burst (Lorimer et al. 2007) was rapidly diminished by the discovery of many such bursts, presumably of terrestrial origin (Burke-Spolaor et al. 2011); but see Keane et al. (2011). Similarly, a long-duration transient found by Levinson et al. (2002) and Gal-Yam et al. (2006) was later traced to a glitch in the VLA on-line data taking system (Ofek et al. 2010), apparently affecting 0.29% of all FIRST survey pointings (Thyagarajan et al. 2011). Finally, our re-analysis (see §3.5) shows that the claim of late time radio emission from neutron star coalescence Nakar & Piran (2011) is premature.

Here we focused on the potentially new class of long duration radio transients reported in B07. We rule out six of the ten transients and cast doubts on some of the remaining ones. However, even with one or two survivors the long duration transients of B07 remain of great interest. First, even with a diminished number of transients

¹³ The rate density of such mergers is poorly constrained. It ranges between 10 to $10^4 \text{ Gpc}^{-3} \text{ yr}^{-1}$ for NS-NS mergers (Phinney 1991; Narayan et al. 1991; Kalogera et al. 2004; Abadie et al. 2010)

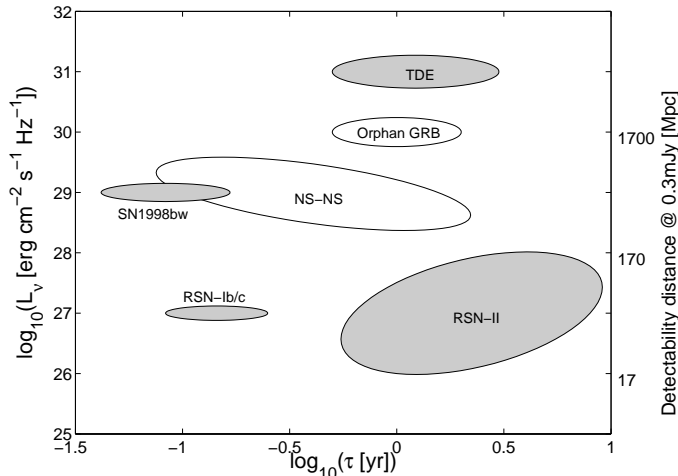


FIG. 7.— Phase space diagram showing the predicted radio luminosity versus evolutionary time scales for several types of long duration radio transient populations. Transparent zones indicate source populations which are typically optically thin, while grey zones indicate source populations that are expected to be optically thick before maximum light, evolving to an optically thin phase at later times. A similar optical version of this figure can be found in Rau et al. (2009) and a more comprehensive figure which includes short duration events is in SKA Memo 97.

the implied areal rate of B07 transients would be comparable to the recently established class of Swift J1644+57 transients. However, *unlike any other long duration radio transient* (to wit, supernovae; active stars; tidal disruption events; gamma-ray burst afterglows, beamed or otherwise) the B07 transients are remarkable for the absence of a quiescent optical counterpart.

The event RT 19920826 survives two independent tests. As such it useful to speculate on the origin of this transient. The absence of an optical (B07) and near IR quiescent source could mean one of two origins. The event is extra-galactic in origin but the host galaxy is faint enough not to have been detected (as does happen for a few percent of long duration GRB host galaxies) or that it is offset from a host galaxy (as in the case for a few short hard bursts; Berger 2009). Alternatively, the event is a Galactic neutron star and we have to then appeal to an optically invisible Galactic (neutron star) population (Ofek et al. 2010).

Clearly, a new survey which can net a dozen of such sources (but brighter!) would help resolve the origin. For the Galactic hypothesis one expect no quiescent counterpart even at HST sensitivity whereas detectable galaxies, in the majority, are expected for the extra-galactic hypothesis.

There are great gains in the discovery of new classes of radio transients but at the same time the path to true success is littered with false starts or easy speculations. The way forward must incorporate the lessons learnt from the false starts. We elaborate on this conclusion below.

To start with we believe that the field of radio transients (at least in the decimeter band) is sufficiently mature that any new survey which just sets an upper limit relative to the known population is of marginal value. Future surveys have to be sufficiently deep and cover large enough sky that success (i.e. detection of a few to many transients) is assured. In our opinion, this means

that a survey should be designed to find at least one or more Swift J1644+57-like transient (Figure 6).

Next, timely and multi-wavelength follow-up is essential. For example, the transients reported in Gal-Yam et al. (2006), Gregory & Taylor (1986) and Bannister et al. (2011a,b) have plausible origins as supernovae and Swift J1644+57-like sources (see Figure 6). However, the lack of timely follow-up or deep multi-wavelength followup of these events preclude us from coming to a definitive conclusion.

Finally, the search should be restricted to sources with a high level of significance. This certainly means paying attention to the large number of beams searched. However, at low thresholds and with large number of beams (cf §3) it would be prudent to set thresholds beyond mere statistical considerations¹⁴. A threshold of 9 or even 10 σ may be appropriate. Alternatively, an immediate verification of a transient by deeper observation or a confirmation by observations at other wavelengths would allow detection of transients closer to threshold.

We start with a discussion of two recent developments. Bell et al. (2011) undertook an ambitious program similar in spirit to B07, namely the investigation of fields surrounding VLA calibrators. Sources with duration between 4 and 40 d were searched for. The total integration time was 435 hr. No transient source in the GHz range with flux greater than 8 mJy was found. The authors place an upper limit to the areal density of 0.032 deg⁻². Assuming $S^{-3/2}$ scaling this areal density is 4.4 deg⁻² and is well above the B07 rate.

The FIRST survey imaged the sky in an hexagonal grid, in which each position in the survey footprint was observed on average 3–4 times (Becker et al. 1995). Thyagarajan et al. (2011) used this fact to construct light curves of sources detected in individual FIRST survey snapshots. They identified 1627 variable candidates with variability exceeding 5 σ . This effort is probably the largest variable and transient survey ever carried out. One disadvantage of such a survey for transient identification is that the co-added images are not much deeper than a single epoch image. This make it hard to tell if an apparent transient source is really a transient or just a variable source that exceeded the detection threshold in one of the epochs.

The limitations discussed above lead us to suggest a new EVLA survey specifically tailored to systematically explore the radio sky. Following that we review a far more ambitious survey – the VAST key project on ASKAP. For the discussion below we will adopt the rates summarized in Table 1. The rates are specified to a flux density of 0.3 mJy and are extrapolated to higher flux densities as $N(> S) \propto S^{-3/2}$.

6.1. EVLA Survey

A moderately ambitious survey with the EVLA can result in great progress. This survey has two virtues. One, the EVLA offers excellent spatial resolution. Next, the EVLA is fully commissioned and is working to specifications.

¹⁴ Separately we caution that the discussion of statistics assumes that the underlying statistics are Gaussian to a very high degree of precision. As noted in the text, the sidelobes of strong sources add an additional source of non-Gaussian noise.

Specifically consider a 100 square degree survey undertaken in the 2–4 GHz band. An integration time of 85 s results in a sensitivity of 0.3 mJy ($10\text{-}\sigma$). A single epoch covering 100 square degrees would require 50 hours. As can be seen from Figure 7 (taken from Table 1) such a survey would have to explore a variety of time scales to probe the emerging classes of transient. Fifteen epochs could reasonably cover the range of a week to years.

Noting the great importance of multi-wavelength imaging data, such a survey would sensibly focus on regions of sky where considerable multi-wavelength data (including radio) exists. One such region is, for example, the SDSS equatorial stripe (Hodge et al. 2011). Furthermore, the high instantaneous sensitivity of the EVLA makes rapid follow up of newly transients possible.

After the first four epochs the reference images will be twice as deep as the survey field. A single new epoch would then yield about ten Swift J1644+57-like sources and four supernovae. Ten such images may find a new example of an SN 1998bw-like event, several clear examples of orphan afterglows and have an excellent chance of finding the first examples of neutron star mergers. We note that these different classes of objects have different characteristics, both in duration (Figure 7) and also in host magnitudes and location with respect to host galaxy. Therefore, it is possible to distinguish between different types of objects.

As note earlier, rapid verification of a transient (either by additional and deeper radio observations or observations at other wavelengths) can reduce the requirement for a high detection threshold. This would then require close rapid reduction – well within the reach of modern computers.

6.2. VAST (ASKAP)

The Variable & Slow Transient (VAST) is an approved key project of ASKAP¹⁵. The VAST-Wide survey aims to survey in the 1.2 GHz band about 10,000 square degrees every day for 2 years. With 40-s integrations the

expected single-epoch rms is 0.5 mJy (VAST Memo#1). Since the survey is planned to be undertaken daily the reference image will be built up quite rapidly.

A comparison of data obtained at a new epoch when compared with the built-up reference image can be expected to detect about six Swift J1644+57-like sources. Type II SN and Swift J1644+57-like sources are relatively long lived and so one could consider averaging the daily images (to say 10 days). The resulting summed data has a sensitivity of 0.16 mJy. The expected number of transients per such summed image is nominally 32 (Type II SN), 82 (Swift J1644+57), 8 (orphan afterglows) and 4 (neutron star coalescences).

To sum up, the dynamic radio sky remains a rich area for exploration. Based on what we know about the areal rates for the *known* transient sources, future synoptic radio imaging surveys are expected to yield substantial numbers of exotic transients. Such surveys will also provide the definitive test for the B07 population.

DAF thanks Jim Condon and Alicia Soderberg for important discussions early on in this project. We thank Steve Croft for a most careful reading of the paper and J. Condon for making several insightful suggestions.

The National Radio Astronomy Observatory is a facility of the National Science Foundation operated under cooperative agreement by Associated Universities, Inc. SRK thanks the Department of Astronomy, University of Wisconsin at Madison for their hospitality. EOO is supported by an Einstein fellowship and NASA grants. SRK's research in part is supported by NASA and NSF. This research has made use of data from the University of Michigan Radio Astronomy Observatory which has been supported by the University of Michigan and by a series of grants from the National Science Foundation, most recently AST-0607523. This research has made use of NASA's Astrophysics Data System.

REFERENCES

- Abadie, J., et al. 2010, *Classical and Quantum Gravity*, 27, 173001
- Bannister, K. W., Murphy, T., Gaensler, B. M., Hunstead, R. W., & Chatterjee, S. 2011, *MNRAS*, 412, 634
- Bannister, K. W., Murphy, T., Gaensler, B. M., Hunstead, R. W., & Chatterjee, S. 2011, *Erratum*, July 2011
- Becker, R. H., White, R. L., & Helfand, D. J. 1995, *ApJ*, 450, 559
- Bell, M. E. 2011, "The Low Frequency Array and the Transient and Variable Radio Sky", PhD thesis, Southampton University.
- Bell, M. E., Fender, R. P., Swinbank, J., et al. 2011, *MNRAS*, 415, 2
- Berger, E. 2009, *ApJ*, 690, 231
- Berger, E., Kulkarni, S. R., Frail, D. A., & Soderberg, A. M. 2003, *ApJ*, 599, 408
- Bloom, J. S., et al. 2009, *arXiv:0902.1527*
- Bloom, J. S., et al. 2011, *Science*, 333, 203
- Booth, R. S., de Blok, W. J. G., Jonas, J. L., & Fanaroff, B. 2009, *arXiv:0910.2935*
- Bower, G. C., Saul, D., Bloom, J. S., Bolatto, A., Filippenko, A. V., Foley, R. J., & Perley, D. 2007, *ApJ*, 666, 346
- Bower, G. C. 2011, *ApJ*, 732, L12
- Bower, G. C., Whysong, D., Blair, S., Croft, S., Keating, G., Law, C., Williams, P. K. G., & Wright, M. C. H. 2011, *arXiv:1107.1517*
- Burke-Spolaor, S., Bailes, M., Ekers, R., Macquart, J.-P., & Crawford, F., III 2011, *ApJ*, 727, 18
- Burrows, D. N., Kennea, J. A., Ghisellini, G., et al. 2011, *Nature*, 476, 421
- Cenko, S. B., Fox, D. B., Moon, D.-S., et al. 2006, *PASP*, 118, 1396
- Cenko, S. B., et al. 2011, *arXiv:1107.5307*
- Chatterjee, S., Murphy, T., & VAST Collaboration 2010, *Bulletin of the American Astronomical Society*, 42, #470.12
- Cotton, W. D. & Perley, R. 2010, *OBIT Development Memo Series No. 17*
- Croft, S., Bower, G. C., Keating, G., Law, C., Whysong, D., Williams, P. K. G., & Wright, M. 2011, *ApJ*, 731, 34
- Croft, S., Tomsick, J. A., & Bower, G. C. 2011, *arXiv:1107.5039*
- Dewdney, P. E., Hall, P. J., Schilizzi, R. T., & Lazio, T. J. L. W. 2009, *IEEE Proceedings*, 97, 1482
- Ellingson, S. W., Clarke, T. E., Cohen, A., et al. 2009, *IEEE Proceedings*, 97, 1421
- Galama, T. J., Vreeswijk, P. M., van Paradijs, J., et al. 1998, *Nature*, 395, 670
- Gal-Yam, A., et al. 2006, *ApJ*, 639, 331
- Gehrels, N. 1986, *ApJ*, 303, 336
- Gehrels, N., Ramirez-Ruiz, E., & Fox, D. B. 2009, *ARA&A*, 47, 567
- Giannios, D., & Metzger, B. D. 2011, *MNRAS*, 1137
- Gregory, P. C., & Taylor, A. R. 1986, *AJ*, 92, 371
- Gregory, P. C., Capak, P., Gasson, D., & Scott, W. K. 2001, *Galaxies and their Constituents at the Highest Angular Resolutions*, 205, 98
- Greisen, E. W. 2003, *Information Handling in Astronomy - Historical Vistas*, 285, 109

¹⁵ <http://www.physics.usyd.edu.au/sifa/vast/index.php>

- Hodge, J. A., Becker, R. H., White, R. L., Richards, G. T., & Zeimann, G. R. 2011, *AJ*, 142, 3
- Johnston, S., Taylor, R., Bailes, M., et al. 2008, *Experimental Astronomy*, 22, 151
- Jonas, J. L. 2009, *IEEE Proceedings*, 97, 1522
- Kalogera, V., et al. 2004, *ApJ*, 601, L179
- Keane, E. F., Kramer, M., Lyne, A. G., Stappers, B. W., & McLaughlin, M. A. 2011, *MNRAS*, 415, 3065
- Kettenis, M., van Langevelde, H. J., Reynolds, C., & Cotton, B. 2006, *Astronomical Data Analysis Software and Systems XV*, 351, 497
- Körding, E., Rupen, M., Knigge, C., Fender, R., Dhawan, V., Templeton, M., & Muxlow, T. 2008, *Science*, 320, 1318
- Kulkarni, S. R., Frail, D. A., Wieringa, M. H., et al. 1998, *Nature*, 395, 663
- Law, N. M., Kulkarni, S. R., Dekany, R. G., et al. 2009, *PASP*, 121, 1395
- Lazio, J. 2008, *Astronomische Nachrichten*, 329, 330
- Levan, A. J., et al. 2011, *Science*, 333, 199
- Levinson, A., Ofek, E. O., Waxman, E., & Gal-Yam, A. 2002, *ApJ*, 576, 923
- Lien, A., Chakraborty, N., Fields, B. D., & Kembell, A. 2011, arXiv:1107.0775
- Lonsdale, C. J., Cappallo, R. J., Morales, M. F., et al. 2009, *IEEE Proceedings*, 97, 1497
- Lorimer, D. R., Bailes, M., McLaughlin, M. A., Narkevic, D. J., & Crawford, F. 2007, *Science*, 318, 777
- Metzger, B. D., et al. 2010, *MNRAS*, 406, 2650
- Metzger, B. D., & Berger, E. 2011, arXiv:1108.6056
- Nakar, E. 2007, *Phys. Rep.*, 442, 166
- Nakar, E., Piran, T., & Granot, J. 2002, *ApJ*, 579, 699
- Nakar, E., & Piran, T. 2011, *Nature*, 478, 82
- Narayan, R., Piran, T., & Shemi, A. 1991, *ApJ*, 379, L17
- Nissanke, S. M., Sievers, J. L., Dalal, N., & Holz, D. E. 2011, arXiv:1105.3184
- Sault, R. J., Teuben, P. J., & Wright, M. C. H. 1995, *Astronomical Data Analysis Software and Systems IV*, 77, 433
- Thyagarajan, N., Helfand, D. J., White, R. L., & Becker, R. H. 2011, arXiv:1107.5901
- Ofek, E. O., Breslauer, B., Gal-Yam, A., Frail, D., Kasliwal, M. M., Kulkarni, S. R., & Waxman, E. 2010, *ApJ*, 711, 517
- Ofek, E. O., & Frail, D. A. 2011, *ApJ*, 737, 45
- Ofek, E. O., Frail, D. A., Breslauer, B., Kulkarni, S. R., Chandra, P., Gal-Yam, A., Kasliwal, M. M., & Gehrels, N. 2011, arXiv:1103.3010
- Oosterloo, T., Verheijen, M. A. W., van Cappellen, W., et al. 2009, *Proceedings of Wide Field Astronomy Technology for the Square Kilometre Array (SKADS 2009)*, 4-6 November 2009, Chateau de Limelette, Belgium.
- Phinney, E. S. 1991, *ApJ*, 380, L17
- Perley, R. A., Schwab, F. R., & Bridle, A. H. 1989, *Synthesis Imaging in Radio Astronomy*, 6,
- Rau, A., et al. 2009, *PASP*, 121, 1334
- Rossi, E. M., Perna, R., & Daigne, F. 2008, *MNRAS*, 390, 675
- Röttgering, H., de Bruyn, A. G., Fender, R. P., et al. 2003, *Texas in Tuscany. XXI Symposium on Relativistic Astrophysics*, 69
- Scott, W. K. 1996, PhD Thesis, *Compact Source Variability at Centimeter Wavelengths*, University of British Columbia
- Soderberg, A. M., et al. 2006, *Nature*, 442, 1014
- Soderberg, A. M., et al. 2010, *Nature*, 463, 513
- Sylvestre, J. 2003, *ApJ*, 591, 1152
- Thyagarajan, N., Helfand, D. J., White, R. L., & Becker, R. H. 2011, arXiv:1107.5901
- Totani, T., & Panaitescu, A. 2002, *ApJ*, 576, 120
- de Vries, W. H., Becker, R. H., White, R. L., & Helfand, D. J. 2004, *AJ*, 127, 2565
- van Velzen, S., Koerding, E., & Falcke, H. 2011, arXiv:1104.4105
- Weiler, K. W., Panagia, N., Sramek, R. A., et al. 2010, *Mem. Soc. Astron. Italiana*, 81, 374
- Welch, J., Backer, D., Blitz, L., et al. 2009, *IEEE Proceedings*, 97, 1438
- Zauderer, B. A., et al. 2011, arXiv:1106.3568
- de Zotti, G., Massardi, M., Negrello, M., & Wall, J. 2010, *A&A Rev.*, 18, 1

APPENDIX

A. PROBABILITY DENSITY FUNCTION OF M TH MAXIMUM

In this section, our goal is to compute the probability density function of the m th highest value of h_j , $j = 1, 2, 3 \dots n$. Let $p(h)$ be the probability density function of h_j with $P(h) = \int_{-\infty}^h p(h)dh$ being the cumulative function. We denote the m^{th} highest value by H_m . Thus the maximum of the series of measurements is H_1 and the minimum value is H_n .

Let $\rho(H_m)$ be the probability density function of $h = H_m$. This means that at least one of the measurements lies in the range $[H_m, H_m + dH_m]$. The probability density for this event is $p(H_m)$. Next, then $n - m$ measurements must lie below this range and $m - 1$ above this range. The probability for any value to be smaller than H_m is $P(H_m)$ and the probability for a value to higher than H_m is $1 - P(H_m)$. This is now a binomial distribution with $n - 1$ total values. Thus the probability density function for H_m is

$$\rho(H_m) = np(H_m) \times \frac{(n-1)!}{(n-m)!(m-1)!} P(H_m)^{n-m} [1 - P(H_m)]^{m-1}. \quad (\text{A1})$$

The first combinatorial factor of n accounts for the possibility that H_m can occupy any position in the sequence. The second combinatorial factor, ${}^{n-1}C_{m-1}$ account for the combinations satisfying the condition that $n - m$ values lie below H_m and $m - 1$ lie above H_m . For both the maximum ($m = 1$) and minimum ($m = n$) Equation A1 simplifies to that expected from basic considerations.

Now let us consider the specific case where h follows Gaussian statistics:

$$p(h) = \frac{1}{\sqrt{2\pi}} \exp(-h^2/2) \quad (\text{A2})$$

where h is normalized in units of σ . The probability that an event is extreme or lies within the range $\pm h$ is

$$\phi(h) = \int_{-h}^{+h} p(h)dh = \frac{2}{\sqrt{\pi}} \int_0^{h\sqrt{2}} \exp(-z^2)dz = \text{erf}(h/\sqrt{2}). \quad (\text{A3})$$

The probability that an event is extreme in only one sense, maximum or minimum, and lies outside the range $[-\infty, h]$ (say) is thus

$$P(h) = \frac{1}{2} \left[1 + \text{erf}\left(\frac{h}{\sqrt{2}}\right) \right] = 1 - \frac{1}{2} \text{erfc}\left(\frac{h}{\sqrt{2}}\right) \quad (\text{A4})$$

where $\text{erfc}(x) = 1 - \text{erf}(x)$.

Consider the case where $n \gg 1$ (say 10^6 or more) and m is small, say 10. Then we can approximate $n - 1 \approx n$, $n - 2 \approx n$, ..., $n - m + 1 \approx n$. Furthermore using the approximation, $(1 - x/n)^n \approx \exp(-x)$, we find in the limiting case where H_m is greater than a few [so that $1 - P(H_m) \ll 1$]:

$$\rho(H_m) = \frac{n}{(m-1)!} p(H_m) \exp \left[-\frac{(n-m)}{2} \operatorname{erfc} \left(\frac{H_m}{\sqrt{2}} \right) \right] \left[\frac{n}{2} \operatorname{erfc} \left(\frac{H_m}{\sqrt{2}} \right) \right]^{m-1}. \quad (\text{A5})$$

B. DISTRIBUTION OF SOURCES WITHIN THE PRIMARY BEAM

Provided that there is sufficient spectral resolution, the response of an interferometer to a source follows the antenna response function (“primary beam”).¹⁶ We will assume that the response function is azimuthally symmetric and specified by $g(\theta)$ where θ is the angular offset from the pointing axis.

Let the areal density of sources with flux density greater than S be a power law, say, $N(> S) \propto S^\alpha$. For Euclidean geometry and most reasonable luminosity functions, $\alpha = -3/2$. Next, we note that detection is really finding sources at a given SNR and above. Fortunately the noise distribution for an interferometric image is uniform. Thus a source with a given flux density will have an SNR, \mathcal{S} , that scales with the primary beam response, $\mathcal{S} \propto Sg(\theta)$. The number of sources above a certain SNR and contained outside an angular radius of θ_0 is

$$n(> \mathcal{S}; > \theta_0) \propto \int_{\theta_0}^{\infty} 2\pi\theta \left(\frac{\mathcal{S}}{g(\theta)} \right)^\alpha d\theta \quad (\text{B1})$$

For the specific case of a Gaussian beam,

$$g(\theta) \propto \exp \left[-\frac{1}{2}(\theta/\theta_*)^2 \right] \quad (\text{B2})$$

where the traditional “full width at half maximum” (FWHM) is $\theta_{\text{FWHM}} = \sqrt{\ln(256)}\theta_*$. Substituting Equation B2 into Equation B1 we obtain

$$n(> \mathcal{S}; > \theta_0) \propto \left(\mathcal{S}/g(\theta_0) \right)^\alpha \quad (\text{B3})$$

Half the sources will be detected outside the radius $\theta_h = \sqrt{-\ln(4)/\alpha}\theta_*$. For $\alpha = -3/2$ we obtain $\theta_h = \sqrt{\ln(16)/3}\theta_* \approx 0.97\theta_*$. The expression $\theta_h = \sqrt{1/6}\theta_{\text{FWHM}} \approx 0.4\theta_{\text{FWHM}}$ is more useful. A plot of $n(> \mathcal{S}; > \theta)$ can be found in Figure 8.

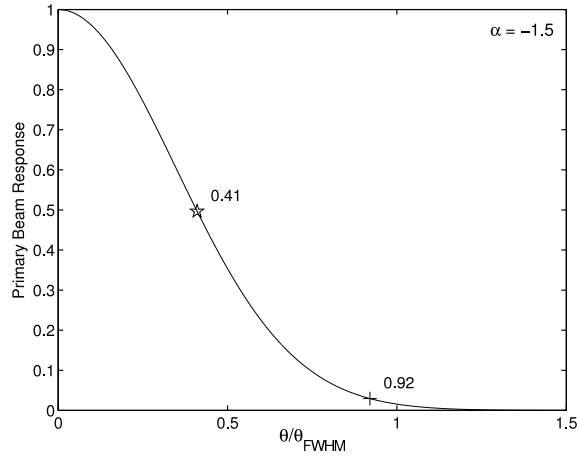


FIG. 8.— The expected distribution of sources above a threshold SNR as a function of $\theta/\theta_{\text{FWHM}}$ from the pointing axis and assuming $\alpha = -3/2$. The response curve is normalized by insisting that the integral of the curve (from $\theta = 0$ to $\theta = \infty$) is unity. Fifty percent of the sources are within $0.41\theta_{\text{FWHM}}$ (marked by a pentagram) and 97% within $0.92\theta_{\text{FWHM}}$ (marked by a cross; at this radius the primary beam gain is only 0.1 relative to that on-axis).

C. UPPER LIMIT FOR A NON DETECTION (POISSON)

It is not unusual to find no source after undertaking a survey. We wish to determine an upper limit to the number of sources that were being searched. The number detected is given by Poisson statistics. The probability of finding r sources is then given by

$$p(r) = \frac{\lambda^r}{r!} \exp(-\lambda) \quad (\text{C1})$$

¹⁶ We assume that the phase center coincides with the pointing axis of the primary antenna.

where λ is the Poisson parameter and equal to $\langle r \rangle$.

Our goal is to determine the maximum value of λ given a non-detection. As the value of λ is increased the probability of detection, by which we mean the probability of detecting one or more events, also increases. This probability is $p(1) + p(2) + \dots$ which we note is $1 - p(0)$. This probability can be set to the desired confidence level, \mathcal{P} and thence

$$\mathcal{P} = 1 - p(0) = 1 - \exp(-\lambda). \quad (\text{C2})$$

The reader with a stronger physical bent may find the complement, $p(0) = 1 - \mathcal{P}$, more appealing. Regardless, we find $\lambda = [3, 4.6, 6.9]$ at a confidence level of [95%, 99%, 99.9%].

D. NUMBER OF INDEPENDENT BEAMS

Here we compute n , the number of independent beams for the VLA data that went into the analysis of B07 and Ofek et al. (2011). For B07, a circular region with a radius of two times the half-power radius was searched for each epoch. The number of independent beams per epoch is the ratio of that area to the area of the synthesized beam in that particular epoch. For individual epochs, this value ranged from as small as 10^3 to as large as 10^6 . The total numbers of independent beams for the 5 and 8.4 GHz data are 9.3×10^7 and 4.5×10^7 , respectively. The smaller number of independent beams for 8.4 GHz are due to the tapering of the visibility data, increasing the typical synthesized beam size at 8.4 GHz.

For Ofek et al. (2011) the search was made for transients in $4.65'$ radius circular region. The FWHM of the synthesized beam is ≈ 4 arc-seconds. Though the goal was 16 epochs per pointing we only achieved an average of 15.7 images. With 141 epochs we derive $n = 1.1 \times 10^7$.